

---

# WOUAF: Weight Modulation for User Attribution and Fingerprinting in Text-to-Image Diffusion Models

---

**Changhoon Kim\***

Arizona State University  
kch@asu.edu

**Kyle Min\***

Intel Labs  
kyle.min@intel.com

**Maitreya Patel**

Arizona State University  
maitreya.patel@asu.edu

**Sheng Cheng**

Arizona State University  
scheng53@asu.edu

**Yezhou Yang**

Arizona State University  
yz.yang@asu.edu

## Abstract

The rapid advancement of generative models, facilitating the creation of hyper-realistic images from textual descriptions, has concurrently escalated critical societal concerns such as misinformation. Traditional fake detection mechanisms, although providing some mitigation, fall short in attributing responsibility for the malicious use of synthetic images. This paper introduces a novel approach to model fingerprinting that assigns responsibility for the generated images, thereby serving as a potential countermeasure to model misuse. Our method modifies generative models based on each user’s unique digital fingerprint, imprinting a unique identifier onto the resultant content that can be traced back to the user. This approach, incorporating fine-tuning into Text-to-Image (T2I) tasks using the Stable Diffusion Model, demonstrates near-perfect attribution accuracy with a minimal impact on output quality. We rigorously scrutinize our method’s secrecy under two distinct scenarios: one where a malicious user attempts to detect the fingerprint, and another where a user possesses a comprehensive understanding of our method. We also evaluate the robustness of our approach against various image post-processing manipulations typically executed by end-users. Through extensive evaluation of the Stable Diffusion models, our method presents a promising and novel avenue for accountable model distribution and responsible use. Our code, data, and demo will be available at: [wouaf.vercel.app](https://wouaf.vercel.app)

## 1 Introduction

Recent advancements in generative models have propelled their proficiency, expanding their repertoire to include not just the generation of photorealistic images [12, 5] but also the synthesis of images from textual prompts [19, 26, 22, 24]. These significant strides have equipped individuals with the capacity to leverage these models to create hyper-realistic images that correspond seamlessly with given textual instructions.

Nonetheless, the escalating prominence of generative models instigates pressing societal apprehensions. A case in point is Deepfake, intentionally crafted to disseminate misinformation, fostering a climate of fake news and political disarray [1, 21, 15]. The gravity of these concerns necessitates calls for governmental intervention to regulate the indiscriminate application of generative models [2, 18]. An immediate, albeit intuitive, countermeasure is the development of fake detection mechanisms [29] capable of discerning real from synthetic content. However, these methodologies could inadvertently serve as additional constraints propelling the creation of increasingly realistic

---

\*These authors contributed equally to this work.

generative models [32, 4]. More significantly, these passive approaches fall short of attributing accountability for the malicious deployment of synthetic images.

A plausible approach to counteracting malicious use involves assigning responsibility for the generated images. One method to realize this is by integrating independent fingerprinting modules (discrete wavelet transform and RivaGAN [33]), which can embed user-specific information into each image post-creation. The open-source Text-to-Image (T2I) project, Stable Diffusion (SD) [24], currently utilizes this technique. Obviously, simply disabling the fingerprinting module can undermine its efficacy.

Can we conduct user attribution without an additional fingerprinting module? In this paper, we present such a model fingerprinting technique to accomplish responsible disclosure. In this approach, the model inventor or distributor modifies the standard generative models based on each user’s distinctive digital fingerprint. By adjusting the generative models, particularly their weights, the resultant content carries a unique fingerprint that can be accurately decoded and traced back to the responsible user.

Model fingerprinting techniques differ depending on the party embedding the fingerprint: the model inventor or the distributor. Inventor-oriented methods [30, 31], require application at the training outset, rendering them incompatible with existing distributor repository models. This constraint necessitates model inventors to balance generation quality and fingerprint embedding. Distributor-oriented methods [14, 20], induce perturbations in the model weights or estimated latent space to achieve fingerprinting. However, within the scope of T2I generative models, estimating learned latent representations becomes particularly challenging due to the expansive space of conditioning text inputs.

In our pursuit of effective model fingerprinting, we put forth a novel distributor-oriented approach, termed as **WOUAF: Weight mODulation for User Attribution and Fingerprinting**. In practical terms, when a model inventor open-sources their work to a model distributor such as Huggingface, the distributor could utilize our proposed method to create a generic version. Upon receiving a download request from an end-user, the distributor can adjust the model weights using our technique and deploy a fingerprinted version to the user, simultaneously registering the user’s fingerprint into their database. In the event of a model’s malicious exploitation, the distributor can decode the fingerprint from the misused image and cross-reference it with their database to identify the responsible user. Consequently, this provides the distributor with an actionable method to counteract malicious uses of the model ( Fig. 1 depicts a comprehensive framework of our methodology.)

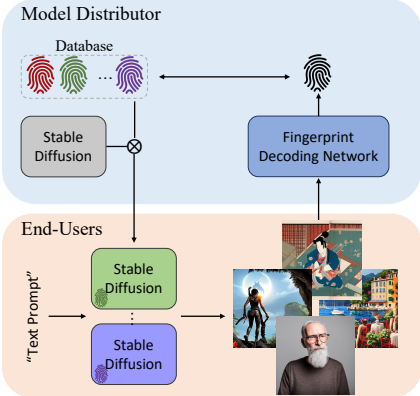


Figure 1: Illustration of user attribution based on our method. Please refer to the main text for detailed descriptions.

Our methodology seamlessly integrates fine-tuning into T2I tasks, leveraging the SD framework. Aligning with previous research, our primary objective is to ensure high attribution accuracy while minimizing degradation in output quality. To achieve this, we employ a mapping network to encode user-specific fingerprints into a discernible fingerprint representation. This is followed by applying a weight modulation method using fingerprint representation. Simultaneously, during the fine-tuning process of the decoder, we train a fingerprint decoder capable of mapping images back to their corresponding user-specific fingerprints (Refer to Sec. 3 for details) .

To validate our approach, we focus on Stable Diffusion model [24], a benchmark within the open-source T2I models. Given that our method necessitates no structural modifications, end-users cannot disable our method. Our evaluation process is four-pronged. Initially, we gauge attribution accuracy and quality, where our method demonstrates near-perfect attribution accuracy while incurring minimal quality degradation. Subsequently, we probe the trade-off between fingerprint length and attribution accuracy. Our method’s secrecy is also scrutinized under two separate scenarios: 1) when a malicious user endeavors to detect the existence of a fingerprint and 2) when a malicious user has a comprehensive understanding of our approach. Finally, we assess the robustness of our method in the face of various image post-processing manipulations that end-users can perform.

**Contributions.** (1) We present a novel distributor-centric model fingerprinting technique (WOUAF) that integrates fine-tuning into T2I tasks, ensuring high attribution accuracy with retained output quality; (2) We devise a practical framework for model distributors to deliver fingerprinted models, enabling user identification in case of model misuse; (3) We rigorously evaluate our method using the Stable Diffusion model, highlighting its attribution accuracy, the trade-off between fingerprint length and attribution accuracy, and robustness against two specific attack scenarios and diverse image post-processings.

## 2 Related Work

**Inventor-oriented Model Fingerprinting.** Yu et al. [31] leveraged a pre-trained deep steganography model to embed fingerprints into the training set for fingerprinted GANs. However, this approach suffers from limited scalability, as it necessitates training a GAN from scratch for each distinct fingerprint. To address this issue, Yu et al. [30] introduced a weight modulation method [10] that directly embeds a user’s fingerprint into the generator’s weights.

Nevertheless, the aforementioned methods have been exclusively examined on GAN-based models and require training from scratch. This raises crucial questions regarding the feasibility of embedding fingerprints into diffusion-based models and the possibility of avoiding training from scratch. These inquiries are particularly pertinent given that state-of-the-art diffusion models, such as those based on latent diffusion, exhibit different structures compared to GANs. By employing fine-tuning for key embedding, model distributors can conveniently integrate fingerprints into pre-trained generative models. This approach allows model inventors to concentrate on the model itself, as they need not consider fingerprints during the training process, which would otherwise introduce further complexity.

**Distributor-oriented Model Fingerprinting.** Kim et al. [14] proposed a technique for achieving user attribution by explicitly incorporating user-specific fingerprints into the generator’s output. While this simplified attribution method allowed for the derivation of sufficient fingerprint conditions, it necessitated a trade-off between the quality of the generated output and attribution accuracy, which was further exacerbated when post-processing was taken into account. To tackle this issue, an approach has been proposed that utilizes subtle semantic variations along latent dimensions as fingerprints, generated by perturbations of eigenvectors in the latent distribution [20]. This method demonstrated an improved balance between generation quality and attribution accuracy. However, its applicability is restricted to unconditional image generation, as eigenvectors are computed by sampling the learned latent representation—a data-specific representation. In the context of conditional image generation, estimating eigenvectors of latent representation becomes challenging due to the vast space of conditions, such as those found in text conditions.

**Stable Diffusion Models.** Our approach is implemented using Stable Diffusion Models (SD) [24], which function within an autoencoder’s latent space. Notably, structural alterations to the model aren’t necessitated for our method.

SD is comprised of two primary components: First, an autoencoder is pretrained on an extensive dataset of images. The encoder,  $\mathcal{E}(\cdot) : \mathbb{R}^{d_x} \rightarrow \mathbb{R}^{d_z}$ , maps an image  $x \sim p_{data}$  into a latent representation  $z = \mathcal{E}(x)$ , while the decoder  $\mathcal{D}(\cdot) : \mathbb{R}^{d_z} \rightarrow \mathbb{R}^{d_x}$  reconstructs the original image from the latent representation, yielding  $x \approx \hat{x} = \mathcal{D}(z)$ . The second component, a U-Net [25] based diffusion model, is trained to generate latent representations within the learned latent space. This diffusion model can be conditioned on class labels or trained text-embeddings. Let  $c(y)$  denote a model mapping a conditioning input  $y$  to a conditioning vector. The SD loss is consequently defined by:

$$L_{SD} := \mathbb{E}_{z \sim \mathcal{E}(x), y, \epsilon \sim N(0,1), t} [\|\epsilon - \epsilon_{\theta}(z_t, t, c(y))\|_2^2], \quad (1)$$

where  $t$  represents the time step,  $\epsilon$  the unscaled noise sample,  $z_t$  the noised  $z$  up to time step  $t$ , and  $\epsilon_{\theta}$  the denoising network. During the inference phase, a random noise is sampled and sequentially denoised using a scheduler with predetermined time steps  $T$  to yield a new image latent,  $z_0$ . This latent code is then transformed into an image via the pretrained decoder,  $\hat{x} = \mathcal{D}(z_0)$ .

## 3 Methods

In this study, we embrace the perspective of a responsible model distributor, equipped to trace the provenance of generated images effectively. Our approach involves fine-tuning existing SD through

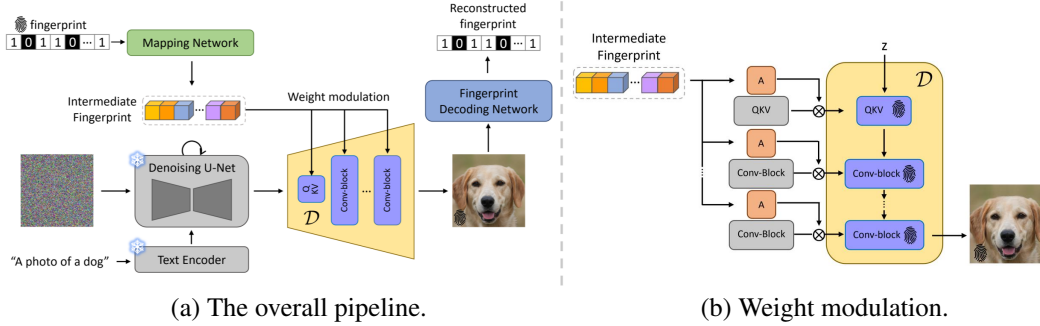


Figure 2: Depiction of our method’s pipeline and weight modulation: (a) The model fingerprinting procedure encompasses encoding via the mapping network and weight modulation, along with decoding through the fingerprint decoding network. (b) Weight modulation of the decoding network  $\mathcal{D}$  to incorporate the fingerprint.

a weight modulation technique, transforming network weights into user-specific weights, hence, embedding fingerprint information into the output images. Concurrently, a fingerprint decoding network is trained during this fine-tuning process to extract fingerprints from images (Fig. 2(a)). Upon deployment, users are provided with their fingerprinted models, while the mapping network and fingerprint decoding network remains exclusively with the model distributor.

### 3.1 User-specific Weight Modulation

Our method is fundamentally based on integrating fingerprints into the parameters of the SD through weight modulation [10, 30].

A user-specific fingerprint is drawn from a Bernoulli distribution with a probability of 0.5, represented as  $\phi \in \Phi := \text{Bern}(0.5)^{d_\phi}$ , where  $d_\phi$  signifies the fingerprint length in bits. We employ a mapping network  $M(\cdot) : \mathbb{R}^{d_\phi} \rightarrow \mathbb{R}^{d_M}$  to convert the sampled fingerprint  $\phi$  into an intermediate fingerprint representation within the  $d_M$  dimension. For modulating each layer in the SD component, we introduce an affine transformation layer,  $A_l(\cdot) : \mathbb{R}^{d_M} \rightarrow \mathbb{R}^{d_j}$ , for all layers  $l$ . This transformation matches the dimensions between  $d_M$  and the  $j$ -th channel in weight  $W \in \mathbb{R}^{i,j,k}$ , where  $i, j, k$  denote input, output, and kernel dimensions, respectively (Refer to Fig. 2(b)). The weight modulation for the  $l$ -th layer is defined as:

$$W_{i,j,k}^\phi = u_j * W_{i,j,k}, \quad (2)$$

where  $W$  and  $W^\phi$  denote the pre-trained and fingerprinted weights respectively,  $u_j = A_l(M(\phi))$  is the scale of the fingerprint representation corresponding to the  $j$ th output channel.

We incorporate fingerprints into the SD by applying weight modulation exclusively to the weights in the decoder  $\mathcal{D}$ . The rationale for not applying modulation to both the diffusion model  $\epsilon_\theta$  and decoder  $\mathcal{D}$ , an approach that mirrors GAN-based models [30], is explained in Sec.4.4.

### 3.2 Training Objectives

Our training architecture comprises two primary objectives. The initial objective is to decode fingerprints from the provided images. We train a ResNet-50 [6]-based fingerprint decoding network,  $\mathcal{F}(\cdot) : \mathbb{R}^{d_x} \rightarrow \mathbb{R}^{d_\phi}$ , as follows:

$$L_\phi = \mathbb{E}_{z \sim E(x), \phi \in \Phi} \sum_{i=1}^{d_\phi} [\phi_i \log \sigma(\mathcal{F}(\mathcal{D}(\phi, z)))_i + (1 - \phi_i) \log(1 - \sigma(\mathcal{F}(\mathcal{D}(\phi, z))))_i], \quad (3)$$

where  $\sigma(\cdot)$  refers to the sigmoid activation function, constraining the output of  $\mathcal{F}$  to the range  $[0, 1]$ . Thus, this loss function effectively amalgamates binary cross-entropy for all bits of the fingerprint.

During training time, fingerprint  $\phi$  is sampled from Bernoulli distribution. However, during distribution, the model distributor initially samples a user-specific fingerprint  $\phi_\alpha$  and subsequently modulates the decoder  $\mathcal{D}$  using  $\phi_\alpha$ . The model the user ultimately receives is the fingerprinted decoder  $\mathcal{D}(\phi_\alpha, \cdot)$ , which solely permits latent input.



The secondary objective endeavors to regularize the quality of outputs. Ideally, this regularization objective inhibits the decoder  $\mathcal{D}$  from compromising image quality while minimizing  $L_\phi$  in (3):

$$L_{quality} = \mathbb{E}_{z \in \mathcal{E}(x), \phi \in \Phi} [\ell(x, \mathcal{D}(\phi, z))], \quad (4)$$

$\ell$  represents the distance metric between original images and fingerprinted images. For practical applications, we utilize perceptual distance [34] to gauge the perceptual difference between  $x$  and  $\mathcal{D}(\phi, z)$ .

The final objective function can be formulated as:

$$\min_{A, M, D, F} \lambda_1 L_\phi + \lambda_2 L_{quality}, \quad (5)$$

where both  $\lambda_1$  and  $\lambda_2$  are set to 1.0. Fundamentally, the loss function aspires to reconstruct fingerprints while maintaining the quality of the generated outputs. To assess the efficacy of our proposed method, we employ attribution accuracy and image quality metrics (Refer to Sec. 4.1 for details).

## 4 Experiments

### 4.1 Experiment Settings

**Datasets.** Our approach was fine-tuned on the MS-COCO [16] dataset, adopting the Karpathy split. For methodological evaluation, we harnessed the test set from MS-COCO and randomly sampled from the LAION-aesthetics [27] dataset. To demonstrate the applicability of our methodology, we further incorporated the ImageNet [3] dataset.

**Evaluations.** User attribution accuracy, an indicator of the consistent incorporation and successful decoding of fingerprints from the output image, is defined as:  $\frac{1}{d_\phi} \sum_{i=1}^{d_\phi} \mathbb{1}(\phi_i = \hat{\phi}_i)$ , where  $\phi$  represents the ground-truth fingerprint and  $\hat{\phi} = \mathbb{1}(\sigma(\mathcal{F}(x_\phi)) > 0.5)$  denotes the estimated fingerprint from the image  $x_\phi$  corresponding to  $\phi$ . Unless otherwise stated, we set  $d_\phi$  to 32 for all experiments (Refer to Sec. 4.2 for further information).

The quality of the generated images is another pivotal evaluation aspect, reflecting our methodology’s efficacy in maintaining image quality whilst embedding the fingerprints. A decline in image quality could dissuade users from downloading and utilizing the model. To numerically represent the quality of outputs, we generated 5,000 images using text prompts from both the MS-COCO test set and LAION aesthetics datasets. We employed the Fréchet Inception Distance (FID)[8] to evaluate image quality, while the Clip-score[7] was utilized to assess the concordance between the text prompt and the generated image.

**Models.** To benchmark attribution accuracy, we utilized the default fingerprinting module in the official SD, denoted as the Discrete Wavelet Transform-based method (DWT) and RivaGAN [33]. Importantly, these modules serve as an upper limit for our method, as they are explicitly designed for fingerprinting, whereas our approach strives to maintain T2I generation capabilities alongside fingerprinting. We also compared the output images from our method with those from the original SD to assess the qualitative changes induced by our approach, providing an upper limit for image quality. For T2I generation, we adopted the Euler scheduler [13] with timestep  $T = 20$ , and the classifier-free guidance scale [9] was set to 7.5 unless otherwise specified.

Finally, we compared our methodology with three variants based on the specific layers chosen for weight-modulation implementation. The first variant (Ours-conv.) applied the modulation solely to the convolutional layers in  $\mathcal{D}$ , reflecting the original proposal for weight modulation [10]. The second variant (Ours-all) implemented weight modulation across all layers in  $\mathcal{D}$ , encompassing self-attention and convolution layers. The last variant applied weight modulation to both the diffusion model  $\epsilon_\theta$  and decoder  $\mathcal{D}$ , similar to the GAN-based method [30]. The reasons for not utilizing this variant throughout all experiments are elaborated upon in Section 4.4.

### 4.2 Fingerprint Capacity

The capacity of our methodology is determined by the maximum count of unique user-specific fingerprints it can sustain without encountering detrimental crosstalk. The primary influencer of this

Table 1: Assessment of attribution accuracy and generation quality. Our method was validated on both the MS-COCO test set and the LAION-aesthetics dataset, which was not employed during our fine-tuning phase. Symbols  $\uparrow/\downarrow$  indicate that higher/lower values are desired, respectively.

Model	Attribution Acc. ( $\uparrow$ )	MS-COCO		Attribution Acc. ( $\uparrow$ )	LAION	
		Clip-score ( $\uparrow$ )	FID ( $\downarrow$ )		Clip-score ( $\uparrow$ )	FID ( $\downarrow$ )
Original SD [24]	-	0.73	24.48	-	0.50	19.67
DWT	0.84	0.74	24.82	0.86	0.50	20.64
RivaGAN [33]	0.99	0.73	24.70	0.99	0.51	20.54
Ours-conv.	0.99	0.73	24.43	0.98	0.51	20.46
Ours-all	0.99	0.73	24.42	0.99	0.51	19.91

Table 2: Assessment of attribution accuracy and generation quality using Imagenet trained models. We validated our method using MS-COCO testset and LAION-aesthetics dataset.  $\uparrow/\downarrow$  indicates higher/lower is desired.

Model	Attribution Acc. ( $\uparrow$ )	MS-COCO		Attribution Acc. ( $\uparrow$ )	LAION	
		Clip-score ( $\uparrow$ )	FID ( $\downarrow$ )		Clip-score ( $\uparrow$ )	FID ( $\downarrow$ )
Ours-conv.	0.99	0.73	24.23	0.99	0.51	19.71
Ours-all	0.99	0.73	24.41	0.99	0.51	19.46

capacity is the dimensionality of the fingerprint dimension ( $d_\phi$ ). However, the task of identifying an optimal  $d_\phi$  is challenging, as a larger  $d_\phi$  paves the way for accommodating more users but simultaneously increases the complexity of effective fingerprint decoding.

To methodically explore this balance, we carried out a thorough analysis, varying the fingerprint dimensionality ( $d_\phi$ ) among a set of predetermined values: 16, 32, 64, 128. Fig. 3 encapsulates the user attribution accuracy corresponding to each  $d_\phi$  value. As illustrated in the figure, there’s a monotonic decline in the attribution accuracy as  $d_\phi$  enlarges.

Interestingly, both our variant models achieved a near-perfect attribution accuracy of 0.99 for  $d_\phi$  values of 16, 32, and 64. However, for  $d_\phi = 128$ , Ours-all variant outperformed Ours-conv. variant. For a balanced comparison with existing methods, we chose  $d_\phi = 32$ , which notably can support a substantial user base exceeding  $4 * 10^9 \approx 2^{32}$ .

An important observation from our experimental procedures is the dependency of training time on  $d_\phi$ . Larger  $d_\phi$  values necessitate extended convergence periods. For example, both our variant models, with  $d_\phi = 32$ , demanded a training duration of 22 hours on a single A100 GPU.

### 4.3 Attribution Accuracy and Image Quality

We conduct a comprehensive evaluation of **WOUAF**, focusing on attribution accuracy and image quality. The assessment involved the MS-COCO test set and the LAION-aesthetics dataset, which was not used during the fine-tuning stage. The results, shown in Table 1, highlight the robust performance of our methodology.

Our variants, Ours-conv and Ours-all, demonstrated superior attribution accuracy compared to DWT, indicating successful decoding of embedded fingerprints from the output images. This strong performance was maintained even when compared to RivaGAN, a specialized fingerprinting model, reinforcing the validity of our approach. Crucially, this level of attribution accuracy was achieved without significant image quality degradation. Deviations in FID scores and Clip-scores compared to the original SD were minimal, indicating negligible impact on output image quality, as further evidenced by qualitative examples in Figure 4. These results underscore the efficacy of **WOUAF** in applications that necessitate reliable fingerprinting while maintaining high-quality image generation. Uncurated image collections can be found in the supplementary material.

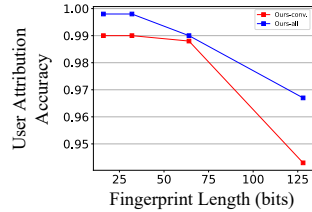


Figure 3: Fingerprint Capacity.

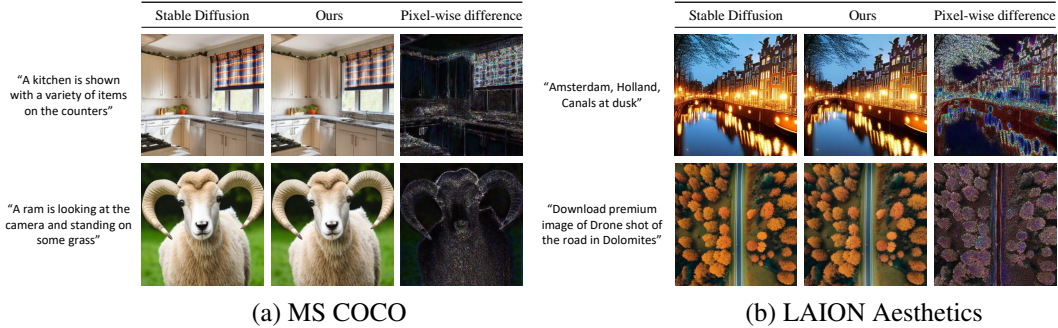


Figure 4: Qualitative comparison of the original and fingerprinted Stable Diffusion models on MS-COCO and LAION aesthetics (Pixel-wise differences  $\times 5$ : they are multiplied by a factor of 5 for better view). We can observe that our method maintains high image quality.

**Evaluating Generalizability Across Datasets.** A key feature of our proposed methodology is its design independence from image-text paired datasets for achieving attribution accuracy. This property imbues it with the potential for broad applicability across a diverse range of contexts. To substantiate this claim, we conducted an experiment in which our variant models were trained exclusively on the ImageNet dataset. We subsequently evaluated the performance of these ImageNet-trained models on the MS-COCO test set as well as a randomly selected portion of the LAION-aesthetics datasets.

The evaluation results, as seen in Table 2, effectively corroborate our assertion. Our methodology demonstrates compelling performance, with both our variants, achieving high attribution accuracy and maintaining image generation quality. These results underscore our method’s independence from the use of text-image paired datasets, thereby establishing its broad applicability in diverse scenarios where reliable fingerprinting and high-quality image generation are required. Additional samples can be found in the supplementary materials.

**Robustness Across Generation Hyperparameters.** In the exploration of model fingerprinting, we acknowledge that users, once in possession of their fingerprinted SD model, may choose to manipulate a variety of hyperparameters in image generation. To ensure the robustness of our proposed approach, we have conducted a comprehensive set of experiments with varying parameters such as the scheduler, number of time steps, and guidance scale. These parameters can significantly influence the quality of images generated, making it essential to thoroughly validate our method across an array of configurations.

To substantiate our approach, we evaluated two widely used schedulers: Euler [13], with time steps in [15, 20, 25], and DDIM [28], with time steps in [45, 50, 55], and guidance scales of 2.5, 5.0, and 7.5. Our findings underscore the resilience and consistency of our method, demonstrating high attribution accuracy regardless of the chosen scheduler or variations in the number of diffusion steps,  $T$ . These results, which align with those depicted in Table 1, are further elaborated upon through detailed tables and figures in supplementary material, providing a more granular understanding of our evaluations.

#### 4.4 Benefits of Finetuning only Decoder

When developing our last variant that incorporates weight modulation into both the diffusion model  $\epsilon_\theta$  and the decoder  $\mathcal{D}$ , we noted that the resultant pipeline demonstrates similarities with the GAN-based method [30]. A direct comparison between ours and GAN based method may not be entirely straightforward, considering the fundamental differences in their training methodologies – GAN-based methods entail training from scratch, whereas our proposed approach leans towards fine-tuning. Nevertheless, both methodologies share a common mechanism: they aim to modulate the weights of the layers instrumental in learning the latent space. This shared characteristic underscores the fundamental objective of optimizing the balance between attribution accuracy and generation quality.

However, our empirical observations suggest that this variant does not consistently achieve commendable performance as an attribution model. Specifically, it appears that this variant can only optimize either attribution accuracy or generation quality, but not both simultaneously. In our experiments, the maximum attribution accuracy achieved by this variant was approximately 89% (Clip-score: 0.68, FID: 63.48). The inherent trade-off observed here further reinforces the challenge of balancing these

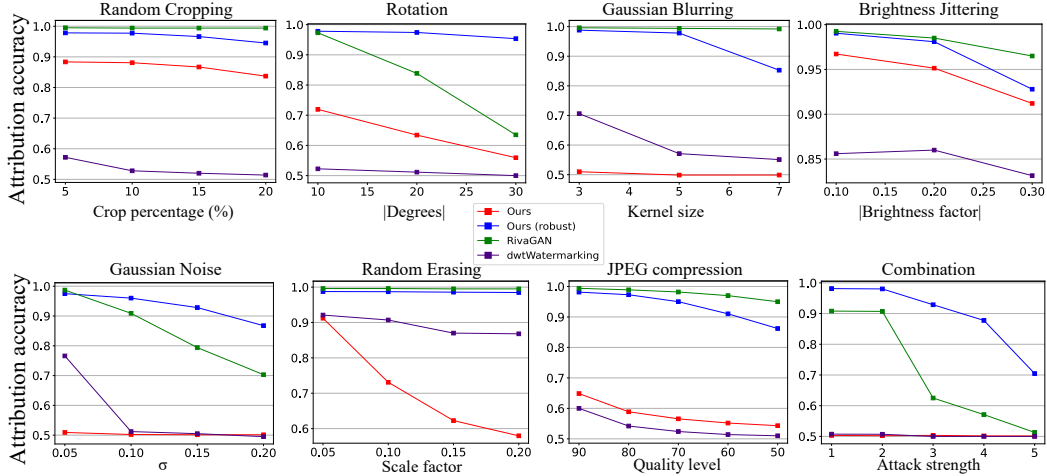


Figure 5: Robust user attribution against image post-processes.

two critical parameters in the context of model fingerprinting techniques. We added sample images of this variant in the supplementary materials.

#### 4.5 Secrecy

The imperceptibility of the embedded fingerprint is of utmost importance, as its detection might enable malicious users to erase or tamper with the fingerprint, thereby confounding the fingerprint decoding network. To evaluate the secrecy of our methodology, we consider two attack scenarios, similar to the settings described in [30].

In the first scenario, the attacker seeks to train a classifier capable of detecting the presence of a fingerprint. To assess this scenario, we employ a ResNet-50 [6] based binary classifier, trained using 10K SD generated images (5K original SD images and 5K fingerprinted SD images). This configuration is deemed valid, as detecting the presence of a fingerprint necessitates using both non-fingerprinted and fingerprinted images in the training set. The binary classifier achieved 98% accuracy in the training stage. Subsequently, we evaluated its performance using an independent set of 5K images from our variant model. As shown in Tab. 3, the user attribution accuracy achieved was only **0.56** for Ours-all variant model, which is almost equivalent to random.

Table 3: User attribution accuracy under attack scenarios on MS-COCO.

Method	Scenario 1	Scenario 2
Ours-conv.	0.662	0.509
Ours-all	<b>0.566</b>	<b>0.501</b>

The second scenario assumes an internal attacker with comprehensive knowledge of our training process, including the training dataset, model structure, fingerprint space, and training details. To validate this, we trained an attacker’s version of our model, following our methodology but employing a different random seed. We then assessed user attribution accuracy by inputting 5K images generated by the attacker’s model into our variants’ fingerprint decoding networks. As demonstrated in Tab. 3, both of our model variants exhibited user attribution accuracies of **0.509** and **0.501**, which are essentially random guesses, and thus dodged the attack.

In conclusion, our findings indicate that our embedded fingerprint, particularly Ours-all variant, is difficult to detect. Moreover, even when an attacker with complete knowledge replicates our methodology, they will not be able to mislead the original fingerprint decoding network.

#### 4.6 Robust User Attribution against Image Post-processes

In this section, we assess the robustness of our approach under scenarios where generated images are subjected to post-processing. These processes may intentionally or unintentionally modify the embedded fingerprint. Given the noteworthy performance of the Ours-all variant in the secrecy evaluation (Section 4.5), we narrow our focus to this particular variant in the subsequent tests.

In line with the protocols detailed in prior works [14, 30, 31, 20], we evaluate the robustness of our model against a variety of image post-processing operations. We examine two versions of our model: the original and a robust variant. The robust variant is constructed by simulating the impact of post-processing, applied with random intensities, prior to feeding data into the fingerprint decoding network,  $\mathcal{F}$ :

$$L_{robust} = \mathbb{E}_{z \sim E(x), \phi \in \Phi} \sum_{i=1}^{d_\phi} [\phi_i \log \sigma(\mathcal{F}(T(\mathcal{D}(\phi, z))))_i + (1 - \phi_i) \log(1 - \sigma(\mathcal{F}(T(\mathcal{D}(\phi, z))))_i)], \quad (6)$$

where  $T(\cdot) : \mathbb{R}^{d_x} \rightarrow \mathbb{R}^{d_x}$  represents the post-processing function. We resolve an optimization problem similar to Eq. (5), but with  $L_\phi$  replaced by  $L_{robust}$ .

In our exploration, we contemplate eight different post-processing techniques: `Cropping`, `Rotation`, `Gaussian Blurring`, `Brightness jittering`, the addition of `Gaussian Noise`, `Erasing`, `JPEG compression`, and a `Combination` of all these techniques. The parameters for these post-processes are designed as follows: For `Cropping`, we use a random crop-out ratio within the range [5%, 10%, 15%, 20%]. `Rotation` involves randomly sampling a degree within the range (-30, 30). For `Gaussian Blurring`, we randomly select a kernel size from [3,5,7]. The `Brightness` factor is randomly sampled within the range (-0.3, 0.3). For `Gaussian Noise`, we add noise with a standard deviation randomly sampled from a uniform distribution  $U[0, 0.2]$ . `Random Erasing` is selected from the range [5%, 10%, 15%, 20%]. `JPEG compression` quality level is selected from [90, 80, 70, 60, 50]. The `Combination` technique randomly selects a subset of these seven post-processing methods with a probability of 0.5.

We evaluated the user attribution accuracy for each post-process during testing, adhering to the pre-defined parameters. For the `Combination` approach, we crafted the attack strength level grounded on the parameters of the other seven procedures. Our robustness test outcomes, delineated in Fig. 5, present a comparative analysis of user attribution accuracy across two benchmark models, our original model, and the robust version of our model. We can observe that our method has a high degree of robustness across various types of real-world attack scenarios.

We noted a consistent trend across all transformation techniques: the user attribution accuracy decreases monotonically with an increase in the strength of post-processing parameters. This observation affirms the challenge posed by post-processing transformations on the task of accurate user attribution.

However, our findings also highlight the efficacy of robust training in mitigating this challenge. Across all cases, we observed a significant improvement in attribution accuracy when we incorporated robust training in our model. This underscores the crucial role of robust training in enhancing the resilience of our fingerprinting method against post-processing transformations. But still, when specifically targeting robust attribution against a `Combination` of post-processes, we noticed a trade-off, as the FID score degraded from 24.42 to 26.85, indicating that the optimization for robustness might unintentionally affect image quality.

Our robust model variant demonstrates a commendable ability to preserve attribution accuracy, frequently matching the performance of established baseline methods under various transformations such as `Rotation`, `Noise`, `Erasing`, and `Combinations`. This suggests a promising capacity of our method to resist diverse post-processing operations without substantially compromising the accuracy of user attribution. It is pertinent to note, however, that while our findings are encouraging, they warrant further investigation and potential enhancements for complete validation and optimization. Further results and visual representations pertaining to both of our model variants can be found in the supplementary materials.

## 5 Conclusion

In this paper, we study stable diffusion based I2T models’ user attribution through weight modulation, achieving near-perfect accuracy without sacrificing quality. Importantly, our WOUAF model’s performance is not reliant on text-image paired datasets and demonstrates robustness against a variety of image generation parameters and secrecy attack scenarios. Our proposed loss function further strengthens the model’s resilience against diverse post-processing techniques. Our findings contribute to the foundation for future research to address challenges presented by generative models at large. **Limitations and future directions:** Despite the encouraging results, the user attribution accuracy of

our model decreases with increased and heavy post-processing transformations, indicating a need for incorporating other advanced weight modulation techniques. We leave testing and analyzing our methodology to other data types such as text, audio, and video as future work, necessitating novel model fingerprinting alterations. Additionally, in-depth exploration and analysis into boosting robustness against post-processing are required.

## **6 Acknowledgment**

This work is partially supported by the National Science Foundation under Grant No. 2038666, No. 2101052, and a grant from Meta AI Learning Alliance. The views and opinions of the authors expressed herein do not necessarily state or reflect those of the funding agencies and employers.

## References

- [1] Ali Breland. The bizarre and terrifying case of the “deepfake” video that helped bring an african nation to the brink. *motherjones*, Mar 2019. URL <https://www.motherjones.com/politics/2019/03/deepfake-gabon-ali-bongo/>.
- [2] Thomas Burri and Fredrik von Bothmer. The new eu legislation on artificial intelligence: a primer. *Available at SSRN 3831424*, 2021.
- [3] Jia Deng, Wei Dong, Richard Socher, Li-Jia Li, Kai Li, and Li Fei-Fei. Imagenet: A large-scale hierarchical image database. In *2009 IEEE conference on computer vision and pattern recognition*, pages 248–255. Ieee, 2009.
- [4] Ricard Durall, Margret Keuper, and Janis Keuper. Watch your up-convolution: Cnn based generative deep neural networks are failing to reproduce spectral distributions. In *Proceedings of the IEEE/CVF conference on computer vision and pattern recognition*, pages 7890–7899, 2020.
- [5] Patrick Esser, Robin Rombach, and Bjorn Ommer. Taming transformers for high-resolution image synthesis. In *Proceedings of the IEEE/CVF conference on computer vision and pattern recognition*, pages 12873–12883, 2021.
- [6] Kaiming He, Xiangyu Zhang, Shaoqing Ren, and Jian Sun. Deep residual learning for image recognition. In *Proceedings of the IEEE conference on computer vision and pattern recognition*, pages 770–778, 2016.
- [7] Jack Hessel, Ari Holtzman, Maxwell Forbes, Ronan Le Bras, and Yejin Choi. Clipscore: A reference-free evaluation metric for image captioning. *arXiv preprint arXiv:2104.08718*, 2021.
- [8] Martin Heusel, Hubert Ramsauer, Thomas Unterthiner, Bernhard Nessler, and Sepp Hochreiter. Gans trained by a two time-scale update rule converge to a local nash equilibrium. In *Advances in Neural Information Processing Systems*, pages 6626–6637, 2017.
- [9] Jonathan Ho and Tim Salimans. Classifier-free diffusion guidance. *arXiv preprint arXiv:2207.12598*, 2022.
- [10] Tero Karras, Samuli Laine, Miika Aittala, Janne Hellsten, Jaakko Lehtinen, and Timo Aila. Analyzing and improving the image quality of stylegan. *arXiv preprint arXiv:1912.04958*, 2019.
- [11] Tero Karras, Miika Aittala, Janne Hellsten, Samuli Laine, Jaakko Lehtinen, and Timo Aila. Training generative adversarial networks with limited data. *Advances in neural information processing systems*, 33:12104–12114, 2020.
- [12] Tero Karras, Samuli Laine, Miika Aittala, Janne Hellsten, Jaakko Lehtinen, and Timo Aila. Analyzing and improving the image quality of stylegan. In *Proceedings of the IEEE/CVF conference on computer vision and pattern recognition*, pages 8110–8119, 2020.
- [13] Tero Karras, Miika Aittala, Timo Aila, and Samuli Laine. Elucidating the design space of diffusion-based generative models. *arXiv preprint arXiv:2206.00364*, 2022.
- [14] Changhoon Kim, Yi Ren, and Yezhou Yang. Decentralized attribution of generative models. In *International Conference on Learning Representations*, 2021.
- [15] Arijeta Lajka. New ai voice-cloning tools ‘add fuel’ to misinformation fire. *AP News*, Feb 2023. URL <https://apnews.com/article/technology-science-fires-artificial-intelligence-misinformation-26cabd20dcacbd68c8f38610fec39f5b>.
- [16] Tsung-Yi Lin, Michael Maire, Serge Belongie, James Hays, Pietro Perona, Deva Ramanan, Piotr Dollár, and C Lawrence Zitnick. Microsoft coco: Common objects in context. In *Computer Vision—ECCV 2014: 13th European Conference, Zurich, Switzerland, September 6–12, 2014, Proceedings, Part V 13*, pages 740–755. Springer, 2014.
- [17] Ilya Loshchilov and Frank Hutter. Decoupled weight decay regularization. *arXiv preprint arXiv:1711.05101*, 2017.



- [18] David McCabe. White house pushes tech c.e.o.s to limit risks of a.i. *New York Times*, May 2023. URL <https://www.nytimes.com/2023/05/04/technology/us-ai-research-regulation.html>.
- [19] Alexander Quinn Nichol, Prafulla Dhariwal, Aditya Ramesh, Pranav Shyam, Pamela Mishkin, Bob McGrew, Ilya Sutskever, and Mark Chen. Glide: Towards photorealistic image generation and editing with text-guided diffusion models. In *International Conference on Machine Learning*, pages 16784–16804. PMLR, 2022.
- [20] Guangyu Nie, Changhoon Kim, Yezhou Yang, and Yi Ren. Attributing image generative models using latent fingerprints. *arXiv preprint arXiv:2304.09752*, 2023.
- [21] Matt Novak. Ai image creator midjourney halts free trials but it has nothing to do with the pope’s jacket. *forbes*, Mar 2023. URL <https://www.forbes.com/sites/mattnovak/2023/03/31/ai-image-creator-midjourney-halts-free-trials-but-it-has-nothing-to-do-with-the-popes-jacket/?sh=ed3f3ec50289>.
- [22] Aditya Ramesh, Prafulla Dhariwal, Alex Nichol, Casey Chu, and Mark Chen. Hierarchical text-conditional image generation with clip latents. *arXiv preprint arXiv:2204.06125*, 2022.
- [23] E. Riba, D. Mishkin, D. Ponsa, E. Rublee, and G. Bradski. Kornia: an open source differentiable computer vision library for pytorch. In *Winter Conference on Applications of Computer Vision*, 2020. URL <https://arxiv.org/pdf/1910.02190.pdf>.
- [24] Robin Rombach, Andreas Blattmann, Dominik Lorenz, Patrick Esser, and Björn Ommer. High-resolution image synthesis with latent diffusion models. In *Proceedings of the IEEE/CVF Conference on Computer Vision and Pattern Recognition (CVPR)*, pages 10684–10695, June 2022.
- [25] Olaf Ronneberger, Philipp Fischer, and Thomas Brox. U-net: Convolutional networks for biomedical image segmentation. In *Medical Image Computing and Computer-Assisted Intervention–MICCAI 2015: 18th International Conference, Munich, Germany, October 5–9, 2015, Proceedings, Part III 18*, pages 234–241. Springer, 2015.
- [26] Chitwan Saharia, William Chan, Saurabh Saxena, Lala Li, Jay Whang, Emily L Denton, Kamyar Ghasemipour, Raphael Gontijo Lopes, Burcu Karagol Ayan, Tim Salimans, et al. Photorealistic text-to-image diffusion models with deep language understanding. *Advances in Neural Information Processing Systems*, 35:36479–36494, 2022.
- [27] Christoph Schuhmann, Romain Beaumont, Richard Vencu, Cade Gordon, Ross Wightman, Mehdi Cherti, Theo Coombes, Aarush Katta, Clayton Mullis, Mitchell Wortsman, et al. Laion-5b: An open large-scale dataset for training next generation image-text models. *arXiv preprint arXiv:2210.08402*, 2022.
- [28] Jiaming Song, Chenlin Meng, and Stefano Ermon. Denoising diffusion implicit models. *arXiv preprint arXiv:2010.02502*, 2020.
- [29] Sheng-Yu Wang, Oliver Wang, Richard Zhang, Andrew Owens, and Alexei A Efros. Cnn-generated images are surprisingly easy to spot... for now. *arXiv preprint arXiv:1912.11035*, 2019.
- [30] Ning Yu, Vladislav Skripniuk, Dingfan Chen, Larry Davis, and Mario Fritz. Responsible disclosure of generative models using scalable fingerprinting. *arXiv preprint arXiv:2012.08726*, 2020.
- [31] Ning Yu, Vladislav Skripniuk, Sahar Abdelnabi, and Mario Fritz. Artificial fingerprinting for generative models: Rooting deepfake attribution in training data. In *Proceedings of the IEEE/CVF International conference on computer vision*, pages 14448–14457, 2021.
- [32] Baiwu Zhang, Jin Peng Zhou, Iliia Shumailov, and Nicolas Papernot. On attribution of deepfakes. *arXiv preprint arXiv:2008.09194*, 2020.
- [33] Kevin Alex Zhang, Lei Xu, Alfredo Cuesta-Infante, and Kalyan Veeramachaneni. Robust invisible video watermarking with attention. 2019.

- [34] Richard Zhang, Phillip Isola, Alexei A Efros, Eli Shechtman, and Oliver Wang. The unreasonable effectiveness of deep features as a perceptual metric. In *Proceedings of the IEEE conference on computer vision and pattern recognition*, pages 586–595, 2018.

## A Training Details

Our proposed method was evaluated utilizing the Stable Diffusion (SD) model [24] (version 2-base), trained specifically for generating images of 512px resolution.

We implemented weight-modulation in alignment with the design specified in the StyleGAN2-ADA [11] source code. Our mapping network  $M$  was designed using multiple fully connected layers, wherein all experiments were conducted using a two-layered configuration. The dimension of the mapping network  $d_M$  was set to be equal to  $4 * d_\phi$  across all experimental setups.

The learning rate was set to  $1e - 4$  and optimized using AdamW [17]. Training was performed over 50,000 iterations with a batch size of 32.

To train models that demonstrated robustness against image post-processing transformations, differentiable post-processes were necessary. To this end, we incorporated the Kornia library [23], which offers a collection of differentiable augmentations.

## B Additional Experimental Results

In addition to the figure in the main paper, we added uncurated images using text-prompt from MS-COCO [16] and LAION Aesthetics [27]. For convenience, we have aligned the subsection names with those in the main manuscript. Unless otherwise specified, all figures were generated using the 'Ours-all' method.

### B.1 Attribution Accuracy and Image Quality

As highlighted in the main manuscript, our methodology has a negligible effect on the original Stable Diffusion’s image quality. Please refer to Fig. 6 for these uncurated images.

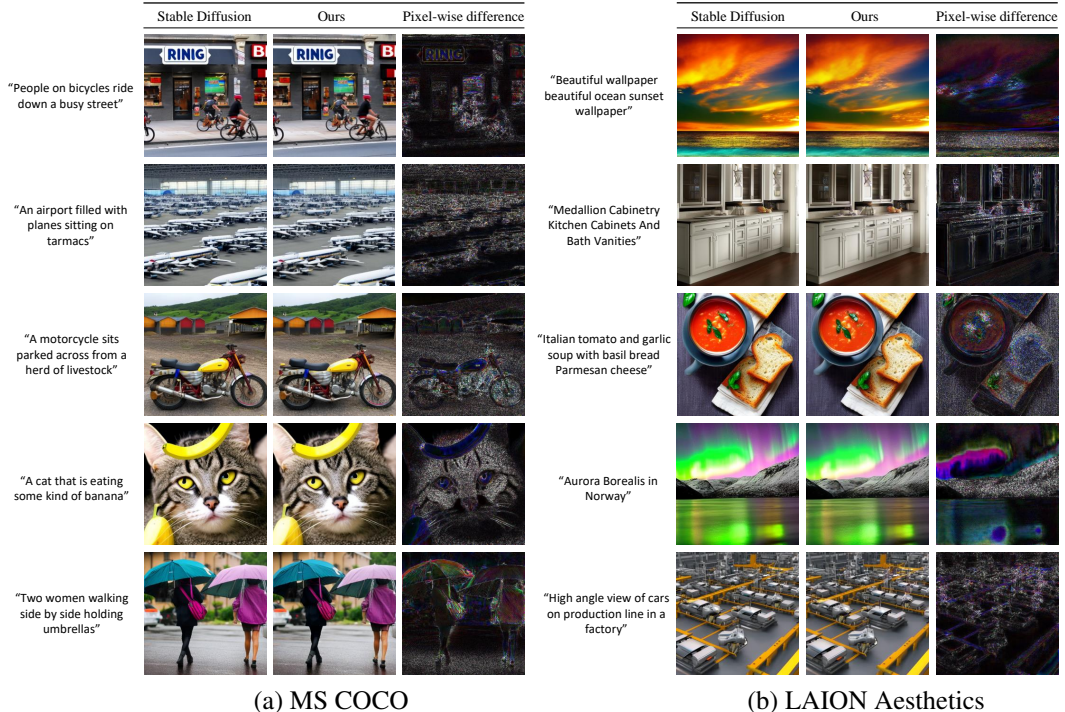


Figure 6: Uncurated images of the original and fingerprinted Stable Diffusion models on MS-COCO and LAION Aesthetics. Pixel-wise differences are multiplied by a factor of 5 for a better view.

## B.2 Evaluating Generalizability Across Datasets

This section presents qualitative results from our technique, which was fine-tuned exclusively using the ImageNet dataset [3]. As underscored in the main manuscript, our model fingerprinting strategy based on weight modulation can be effectively employed using only an image-based dataset. Fig. 7 provides a visual representation of these images.

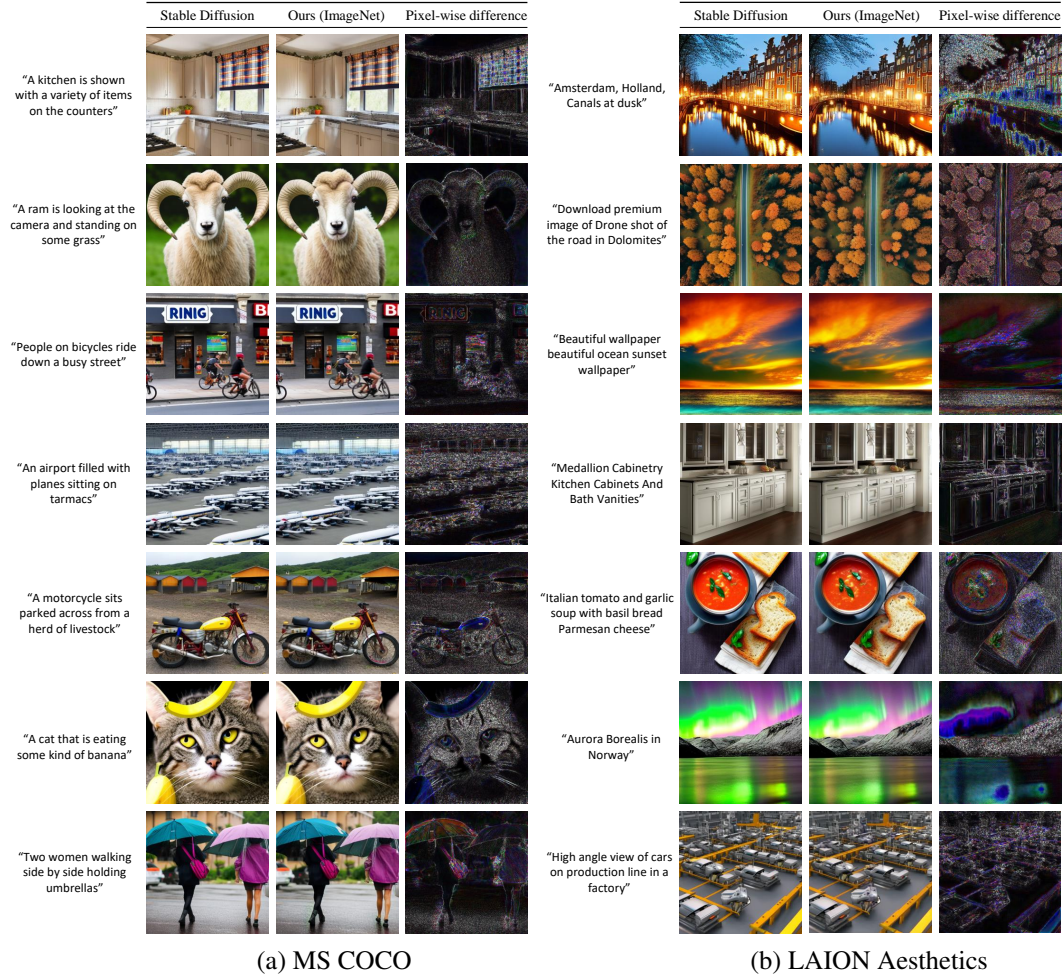


Figure 7: Qualitative comparisons of the original and fingerprinted Stable Diffusion models that were fine-tuned using only the ImageNet dataset. Pixel-wise differences are multiplied by a factor of 5 for a better view.

## B.3 Robustness Across Generation Hyperparameters

In accordance with the details provided in the primary manuscript, we subjected our methodology to evaluation employing two widely accepted schedulers: Euler [13], featuring time steps at intervals of [15, 20, 25], and DDIM [28], operating at time steps in [45, 50, 55]. Along with these, we also incorporated classifier-free guidance scales [9] at 2.5, 5.0, and 7.5.

Echoing the discussions in the main paper, the data in Tables 4 and 5 corroborate the near perfect attribution accuracy achieved by our method. Furthermore, the absence of significant deterioration in quality metrics reaffirms the resilience of our approach in the face of diverse generation hyperparameters (Refer to Fig. 8 and Fig. 9).

Table 4: Assessment of attribution accuracy and generation quality using Euler and DDIM scheduler with different time steps on MS-COCO. We fixed classifier-free guidance scale [9] to **7.5**.  $\uparrow/\downarrow$  indicates higher/lower is desired.

Model	Steps	Euler [13]		FID ( $\downarrow$ )	Steps	DDIM [28]		FID ( $\downarrow$ )
		Attribution Acc. ( $\uparrow$ )	Clip-score ( $\uparrow$ )			Attribution Acc. ( $\uparrow$ )	Clip-score ( $\uparrow$ )	
original SD [24]	20	-	0.73	24.48	50	-	0.73	23.33
Ours-conv.	15	0.99	0.73	24.63	45	0.99	0.73	23.28
	20	0.99	0.73	24.43	50	0.99	0.73	23.35
	25	0.99	0.74	24.14	55	0.99	0.73	23.31
Ours-all	15	0.99	0.73	24.65	45	0.99	0.73	23.34
	20	0.99	0.73	24.42	50	0.99	0.73	23.29
	25	0.99	0.73	24.11	55	0.99	0.73	23.26

Table 5: Assessment of attribution accuracy and generation quality on different classifier-free guidance scales [9] using MS-COCO. We fixed the scheduler and time steps to Euler for **20** steps and DDIM for **50** steps.  $\uparrow/\downarrow$  indicates higher/lower is desired.

Model	Scheduler	Guidance Scale [9] 2.5			Scheduler	Guidance Scale [9] 5.0		
		Attribution Acc. ( $\uparrow$ )	Clip-score ( $\uparrow$ )	FID ( $\downarrow$ )		Attribution Acc. ( $\uparrow$ )	Clip-score ( $\uparrow$ )	FID ( $\downarrow$ )
Ours-conv.	Euler	0.99	0.72	18.63	Euler	0.99	0.73	21.91
	DDIM	0.99	0.72	18.35	DDIM	0.99	0.73	20.78
Ours-all	Euler	0.99	0.71	18.64	Euler	0.99	0.73	21.89
	DDIM	0.99	0.71	18.31	DDIM	0.99	0.73	20.68

#### B.4 Benefits of Finetuning only Decoder

In this section, we present qualitative outcomes resulting from the joint fine-tuning of the Stable Diffusion model’s components, diffusion model  $\epsilon_\theta$  and decoder  $\mathcal{D}$ . As accentuated in the primary manuscript, our training protocol achieved an accuracy of 89%, however, it resulted in a noticeable deterioration in the quality metrics (Clip-score: 0.68, FID: 63.48). Figure 10 provides a visual affirmation of these quantitative results.



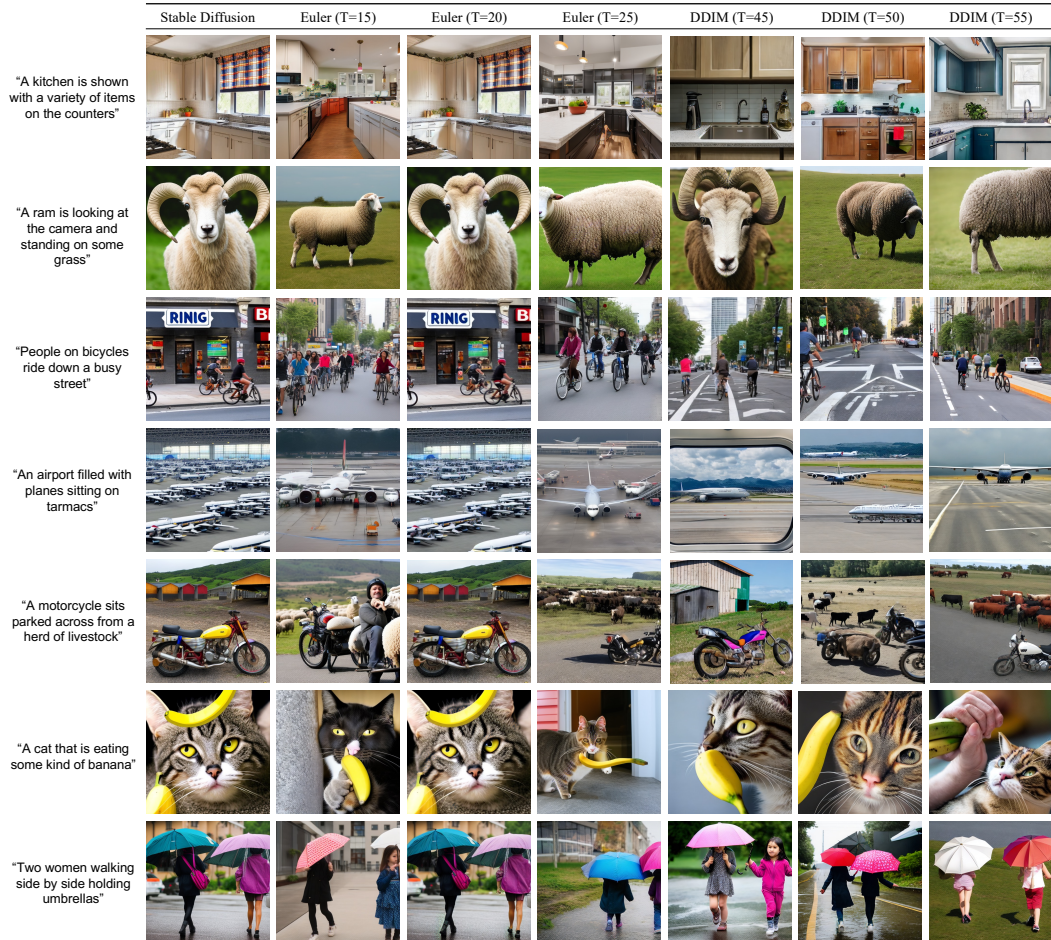


Figure 8: Qualitative results obtained using the Euler and DDIM schedulers with varying time steps on the MS-COCO dataset. We maintained a constant classifier-free guidance scale [9] at **7.5**. Each column corresponds to the 'Ours-all' rows in Table 4.

### B.5 Robust User Attribution against Image Post-processes

As detailed in the main manuscript, we show the robust attribution accuracy results of our variants (Ours-all and Ours-conv.), as depicted in Fig. 11. A comparative analysis of our robust variants, Ours-all and Ours-conv., indicates comparable attribution accuracy. However, a slight overall superiority can be attributed to the Ours-all variant.

We also present a comprehensive evaluation of quality metrics, illustrating the impact of our robust user attribution training against individual image post-processing methods (Refer to Tab. 6 and Tab. 7). The results indicate that our robust fine-tuning generally maintains the image quality with minimal perturbations. To substantiate this, we provide a representative image created by our robust model under a JPEG attack (See Fig. 12). Nonetheless, a Combination attack results in a visible degradation of image quality. Consequently, we provide images generated by our model under a Combination attack (Fig. 13). We also provide images by Ours-conv. model under the two types of attacks in Fig. 14.

Contrary to other figures (Fig. 6, 7, 12), Fig. 13 demonstrates the introduction of significant noise when the model is fortified to withstand a Combination attack. As elucidated in the main manuscript, this introduces a trade-off: the enhanced robustness against the Combination attack is accompanied by a noticeable decline in image quality.







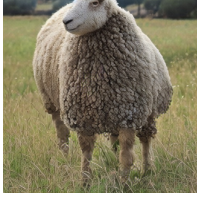

















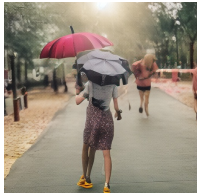



	Euler (s=2.5)	Euler (s=5.0)	DDIM (s=2.5)	DDIM (s=5.0)
"A kitchen is shown with a variety of items on the counters"				
"A ram is looking at the camera and standing on some grass"				
"People on bicycles ride down a busy street"				
"An airport filled with planes sitting on tarmacs"				
"A motorcycle sits parked across from a herd of livestock"				
"A cat that is eating some kind of banana"				
"Two women walking side by side holding umbrellas"				

Figure 9: Qualitative results produced by applying different classifier-free guidance scales [9] on the MS-COCO dataset. The scheduler and time steps were held constant at Euler for **20** steps and DDIM for **50** steps. Each column aligns with the 'Ours-all' rows in Table 5.



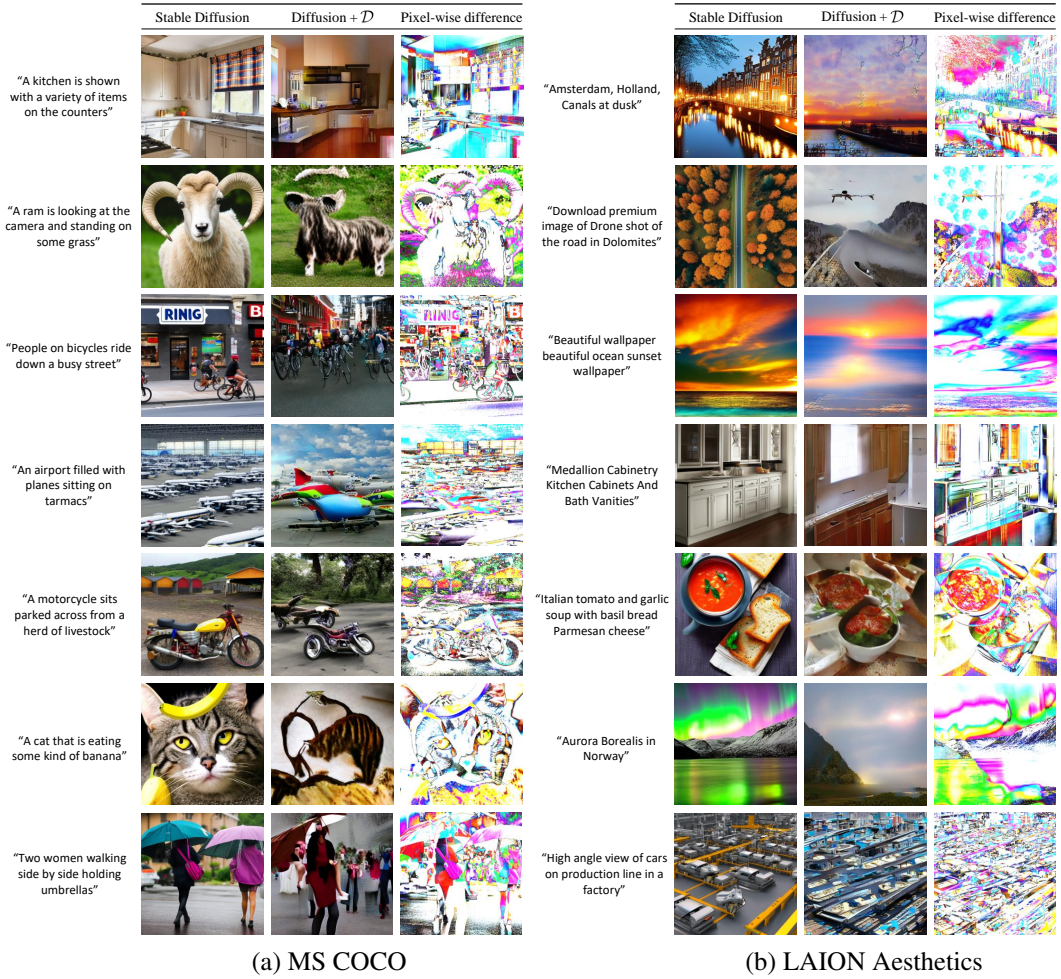


Figure 10: Qualitative results of the original and fingerprinted Stable Diffusion models on MS-COCO and LAION Aesthetics. When fine-tuning the SD model's  $\epsilon_\theta$  and  $\mathcal{D}$  together, there are significant quality drops. Pixel-wise differences are multiplied by a factor of 5 for a better view.

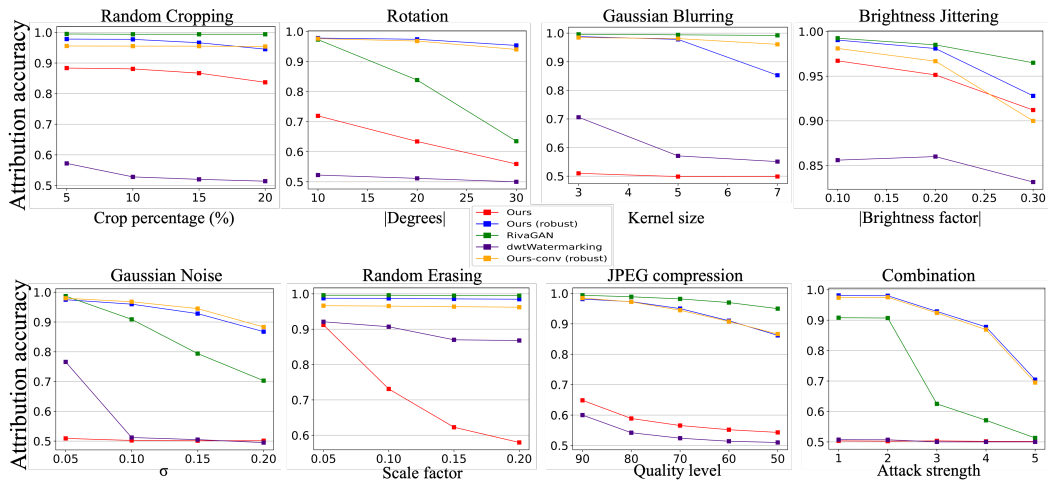


Figure 11: Robust user attribution against image post-processes.

Table 6: FID [8] scores using MS-COCO after robust training. Lower is desired.

Model	Crop	Rotation	Blur	Brightness	Noise	Erasing	JPEG	Combi.
Ours-conv. (robust)	24.02	24.05	23.80	24.14	23.96	24.16	24.42	26.80
Ours-all (robust)	24.35	23.92	24.18	24.54	24.24	24.48	24.41	26.85

Table 7: CLIP scores [7] using MS-COCO after robust training. Higher is desired.

Model	Crop	Rotation	Blur	Brightness	Noise	Erasing	JPEG	Combi.
Ours-conv. (robust)	0.716	0.717	0.716	0.716	0.712	0.717	0.714	0.702
Ours-all (robust)	0.719	0.717	0.718	0.718	0.710	0.718	0.716	0.704

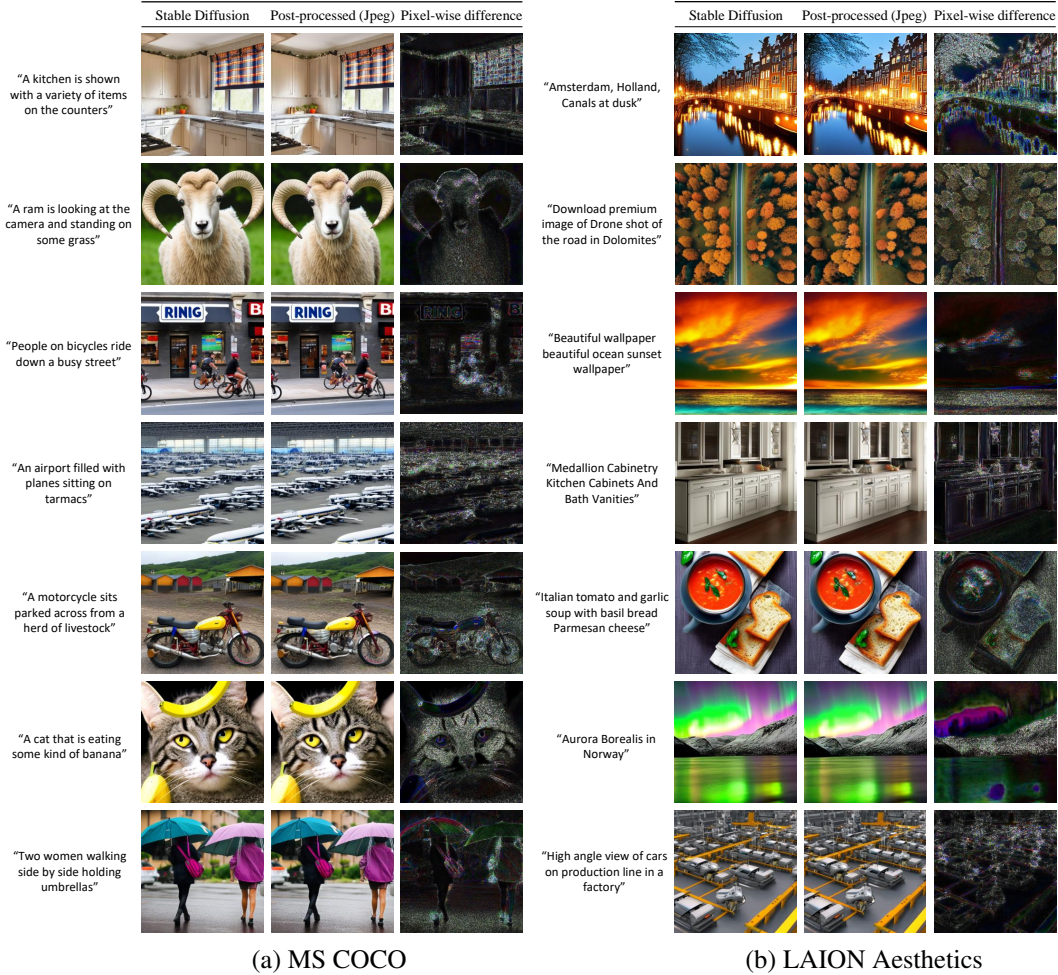
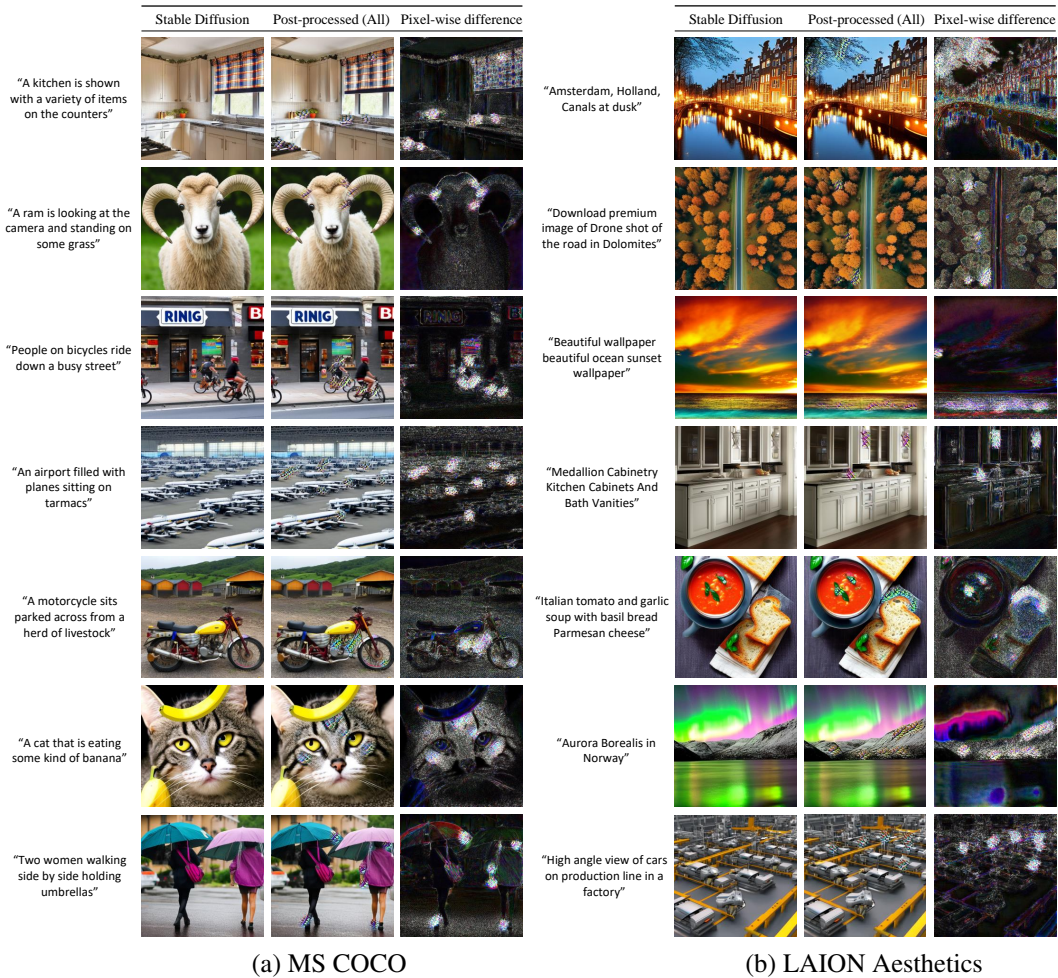


Figure 12: Qualitative results of the original and fingerprinted Stable Diffusion models on MS-COCO and LAION aesthetics. Our fingerprinted model is trained by simulating JPEG compression during training. Pixel-wise differences are multiplied by a factor of 5 for a better view.





(a) MS COCO

(b) LAION Aesthetics

Figure 13: Qualitative results of the original and fingerprinted Stable Diffusion models on MS-COCO and LAION aesthetics. Our fingerprinted model is trained by simulating all the combinations of the post-processing during training. Pixel-wise differences are multiplied by a factor of 5 for a better view.



Figure 14: Qualitative results of the original and fingerprinted Stable Diffusion models (Ours-conv.) on MS-COCO. Pixel-wise differences are multiplied by a factor of 5 for a better view.